Dynamical properties of Ultraluminous Infrared Galaxies II: Tracing the evolution of the stellar kinematics during the Ultraluminous phase(s) of local mergers

K. M. Dasyra[1], L. J. Tacconi[1], R. I. Davies[1], T. Naab[2], R. Genzel[1], D. Lutz[1], E. Sturm[1], A. J. Baker[3,4], S. Veilleux[4], D. B. Sanders[5], A. Burkert[2]

ABSTRACT

We present results from our Very Large Telescope large program to study the dynamical evolution of local Ultraluminous Infrared Galaxies (ULIRGs) and QSOs. Expanding previous studies by Genzel et al. (2001) and Tacconi et al. (2002), our data now consist of high resolution, long-slit H- and K-band spectra of 54 ULIRGs. This paper mainly presents the kinematics of sources that have coalesced into a single nucleus. The stellar kinematics, extracted from the CO rovibrational bandheads in our spectra, indicate that ULIRG remnants are dynamically heated systems with a mean dispersion of 157 $\mathrm{km\,s^{-1}}$. The combination of kinematic, structural, and photometric properties of the remnants indicate that they mostly originate from major encounters (in agreement with Dasyra et al. 2006) and that they result in the formation of dispersion-supported systems (elliptical galaxies of the order $\sim 10^{10}$-$10^{11}\,M_{\odot}$). Placing ULIRGs on the fundamental plane of early-type galaxies indicates that the end products of ultraluminous mergers are typically less massive and extended than giant ellipticals (in good agreement with Genzel et al. 2001 and Tacconi et al. 2002). Converting the host dispersion into black hole mass with the aid of the $M_{\mathrm{BH}} - \sigma$ relation yields black hole mass estimates of the order 10^7- 10^8 $M_{\odot}$ and high accretion rates (of Eddington efficiencies often > 0.5).

Subject headings: galaxies: formation — galaxies: kinematics and dynamics — infrared: galaxies — ISM: kinematics and dynamics —

[1]Max-Planck-Institut für extraterrestrische Physik, Postfach 1312, 85741, Garching, Germany

[2]Universitätssternwarte, Scheinerstr. 1, 81679, München, Germany

[3]Jansky Fellow, National Radio Astronomy Observatory

[4]Department of Astronomy, University of Maryland, College Park, MD 20742, USA

[5]Institute for Astronomy, University of Hawaii, 2680 Woodlawn Drive, Honolulu, HI 96822, USA

1. Introduction

Galaxy mergers, the frequency of which increases with redshift (Kauffmann & White 1993; Le Fèvre et al. 2000), are considered a key mechanism in driving galaxy evolution. In the local Universe, the best laboratories for studying violent merging events (believed to be the probable analogs of high-redshift mergers) are the ultraluminous infrared galaxies (ULIRGs). ULIRGs have a high luminosity output in the infrared (IR), which is greater than $10^{12} L_{\odot}$ and comparable to the bolometric luminosities of QSOs.

A plethora of studies indicates that ULIRGs transform gas-rich disks into ellipticals (Es) through merger-induced dissipative collapse (Kormendy & Sanders 1992; Mihos & Hernquist 1996). The large molecular gas concentrations in the central kpc regions of ULIRGs (e.g. Downes & Solomon 1998; Bryant & Scoville 1999) have densities comparable to stellar densities in ellipticals. Kim et al. (2002) and Veilleux et al. (2002) have analyzed the structural parameters of a sample of 118 ULIRGs that have 60 μm flux greater than 1 Jy (hereafter the 1 Jy sample). They find that most (73%) are well-fit by an elliptical-like $r^{1/4}$ light profile. Similar findings on the near-IR light distributions of ULIRGs were reported by Scoville et al. (2000). Genzel et al. (2001) and Tacconi et al. (2002) have made high-resolution near-infrared (NIR) spectroscopic measurements of the stellar dynamics of small samples consisting mostly of fully-merged ULIRGs. They conclude that ULIRGs resemble intermediate mass ellipticals/lenticulars with moderate rotation, in their velocity dispersion distribution, their location in the fundamental plane (FP; e.g., Djorgovski & Davis 1987; Dressler et al. 1987) and their distribution of the rotational/dispersion velocity ratio. Together, these results suggest that ULIRGs form moderate mass ellipticals (of stellar mass $\sim 10^{11}$ $M_{\odot}$).

One way to investigate the physical details and the evolution of ULIRGs is to determine the kinematic and structural properties of the merging (or interacting) galaxies in different merger phases. We therefore conducted a European Southern Observatory (ESO) large program[1] that traces the host dynamics of a large sample of ULIRGs (spanning wide ranges of merger phase and infrared luminosity) through NIR spectroscopy. Our study extends the previous work by Genzel et al. (2001) and Tacconi et al. (2002) by including a wider range of ULIRG merger phase and luminosity. In Dasyra et al. (2006, hereafter Paper I) we analyzed those ULIRGs that are in a merger phase later than the first encounter but prior to nuclear coalescence, and hence, show more than one nucleus in the NIR acquisition images. In this paper we present results from those ULIRGs that have coalesced and show a single nucleus in our images, the so-called remnants. We compare the stellar kinematic properties

[1] 171.B-0442 (PI Tacconi)

of binary ULIRGs and ULIRG remnants to study the evolution of ultraluminous mergers.

Some of the ULIRGs presented in this study may in fact be binary sources very close to coalescence that have small projected nuclear separations; such sources cannot always be resolved (or kinematically disentangled) due to instrumental angular resolution constraints. At redshifts typical for the sources in our sample, the angular resolution achieved implies that any unresolved systems will have nuclear separations smaller than 1 kpc. Merger simulations (e.g. Mihos 2000) have shown that by the time the individual nuclei are separated by $\lesssim$ 1 kpc, the stellar kinematics have almost reached their relaxation values. Therefore, the dynamical properties of all the sources we classify as remnants are representative of those at dynamical equilibrium.

This paper is arranged as follows. We briefly summarize the observations and present our data in § 2. After studying how the kinematic properties of the merging galaxies evolve with time in § 3, we investigate potential ultraluminous merger end products in § 5. We then focus on the black hole properties of ULIRGs: an analysis of the evolution of the $M_{\rm BH}$-σ relation during the merger in § 6 is followed by a discussion of the nuclear activity implied by our data in § 7. Finally a summary is presented in § 8.

2. Observations and data

We have obtained near-infrared, long-slit spectroscopic data using the ISAAC spectrometer (Moorwood et al. 1998) mounted on the Antu telescope unit of the Very Large Telescope (VLT). Together with the sources presented in Genzel et al. (2001) and Tacconi et al. (2002), we now have high resolution NIR spectra of 54 ULIRGs and 12 QSOs. In this paper, we complete the presentation of the ULIRGs in our program by studying the kinematics of mergers in an ultraluminous post-coalescence phase (ULIRG remnants). The stellar kinematics of the QSOs will be presented in a forthcoming paper (Dasyra et al. 2006, in preparation).

We present new data for 17 of the 30 sources listed in Table 1. According to the NICMOS imaging of Scoville et al. (2000), Mrk 273 and IRAS 15250+3609 have a projected nuclear separation of 0.7 kpc and need to be treated as remnants. The same applies for the resolved binary Arp 220 with a projected nuclear separation of 0.3 kpc (Genzel et al. 2001). The resolved binary NGC 6240 has a nuclear separation of 1.4 kpc, which exceeds (but is very close to) the threshold of 1 kpc that we set to define our remnants. Since the stellar kinematics of its two components are very similar (identical within the error bars: Tecza et al. 2000;Genzel et al. 2001), a strict classification of this source is not straightforward.

Furthermore, the observed stellar kinematics are believed to be affected by localized motions of self-gravitating internuclear gas or even projection effects (Tecza et al. 2000;Genzel et al. 2001). For these reasons, we opt to exclude NGC 6240 from any statistical analyses in this paper.

According to the recent NICMOS imaging of Veilleux et al. (2006), a second (fainter) source is present north-east of IRAS 00456-2904, at a projected nuclear separation of 20.7 kpc. Whether this is a second nucleus at the same redshift is not spectroscopically confirmed. The imaging analysis of Veilleux et al. (2006) shows that the (bright) south-west nucleus is a late-type galaxy while the north-east source is of ambiguous type. These findings indicate that IRAS 00456-2904 is probably in an early-interaction phase and should be classified as a binary system.

Taking the above into account we find that of the 54 ULIRGs observed, 30 are merger remnants, 23 are (binary) progenitors, and 1 (IRAS 00199-7426: Duc et al. 1997; Paper I) may be a multiple-interaction system.

A detailed description of the criteria for the sample selection, the wavelength range of the observations, and the instrument mode used is given in Paper I. The pixel scale was 0.146″per pixel. The total exposure times, and the slit position angles for each ULIRG remnant are presented in Table 1. If the position angle of the major axis of rotation could not be identified (e.g. from the elongation of the stellar disk), the slits were typically placed at 0° and 90°. The redshift range of the sources in the present sample is $0.042 < z < 0.268$ (see Table 1). No sources are observed for the redshift sub-range $0.163 < z < 0.199$, since the CO bandheads are then shifted into wavebands of high atmospheric absorption.

As in Paper I, we derive the structural parameters of the sources that do not have high-resolution NIR imaging (e.g. Hubble Space Telescope NICMOS) data by fitting ellipses to our H-band acquisition images (with the aid of the SExtractor package; Bertin & Arnouts 1996). The half-light radius $R_{\rm eff}$, the ellipticity, and the angle ϕ_α between the major axis of rotation and the position angle of the first slit are presented in Table 2 for each source. To convert all angular distances into linear sizes we use a H_0=70 km s^{-1} Mpc^{-1}, Ω_m=0.3, $\Omega_{\rm total}$=1 cosmology.

The extraction of the stellar central velocity dispersion σ and rotational velocity $V_{\rm rot}$ from the spectra follows the method presented in Paper I. It is performed using the Fourier quotient technique (Bender 1990); this method provides the intrinsic line-of-sight (LOS) velocity profile along any given aperture. To this we fit a Gaussian to determine the average LOS radial velocity and velocity dispersion. The central aperture spectrum of each source (combined over the two slits and shifted to restframe) is displayed in Fig. 1. The stellar

template, an M0III giant (HD 25472), is overplotted with a dashed line after being convolved with the Gaussian that best simulates the LOS broadening function.

The stellar kinematic results (central velocity dispersion and rotational velocity) can be found in Table 3. From the LOS rotational velocity, $V_{\rm rot}$(LOS) measured along each slit, we calculate the observed rotational velocity $V_{\rm rot}(obs)$ by correcting for the angular deviation of the slit from the major axis of rotation (as $V_{\rm rot}(obs) = V_{\rm rot}[{\rm LOS}]/cos[\phi_\alpha]$), and by averaging the result over the slits. The value of the observed rotational velocity is given in Table 3 and is related to the actual rotational velocity $V_{\rm rot}$ as $V_{\rm rot}({\rm obs}) = V_{\rm rot} sin(i)$. To correct for the inclination i of the stellar disks, we used the mean value of $sini$ (0.5) observed for disk-like galaxies on the sky. The conversion of ellipticity into i for the remnants is very uncertain since their stellar disks are dynamically hot (due to the advanced phase of the merger).

3. Evolution of the galaxy kinematics

The mean stellar velocity dispersion of the remnants of ultraluminous mergers presented in Table 3, including Arp 220, is 157 $\rm km\,s^{-1}$, with a dispersion of $\pm$40 $\rm km\,s^{-1}$. The velocity dispersion of ULIRGs in a merger phase prior to coalescence is 143 ($\pm$ 21) $\rm km\,s^{-1}$, when IRAS 00456−2904(SW) is added to the sources of Paper I.

The pre- and post- coalescence dispersion distributions are shown in Fig. 2. While the difference in the mean of the two distributions is small, the remnant velocity dispersion distribution has a larger variance and a tail at the high-σ end, the statistical significance of which needs to be quantified.

To investigate whether the two distributions are independent, we created a Monte Carlo code, beginning with the assumption that the two distributions are drawn from the same parent population. We used 10^6 points to simulate a Gaussian parent distribution that fits the combined pre- and post- coalescence ULIRG dispersion measurements. From the parent distribution, we selected random points to generate two (artificial progenitor/remnant) subsamples, each having a number of elements equal to that of the corresponding real population. We then calculated the difference in the mean of the two generated samples and the difference in the variance between each real population and the (corresponding) generated sample. We repeated this procedure for 10000 iterations and found that the probability of the difference in the mean of the two generated samples to be equal or greater than the measured one (14 $\rm km\,s^{-1}$) is 0.051. The probability p that the variances of both generated samples ($\sigma^2_{\rm gen,1}$ and $\sigma^2_{\rm gen,2}$ respectively) are greater than those measured (or $p[\sigma_{\rm gen,1} > 21\,{\rm km\,s^{-1}}] * p[\sigma_{\rm gen,2} > 40\,{\rm km\,s^{-1}}]$) is 0.011. In other words, while the probability

that the means of the observed distributions are independent is marginally significant, 94.9% (meaning that the means are 2 Gaussian sigma apart), the probability that their variances are independent is significantly high, 98.9%.

This result favors the hypothesis that the apparent kinematic evolution is real rather than an artifact of limited-number statistics. From the definition of a normal distribution's standard error, we estimate that we would still need twice as many measurements to reach a 3 Gaussian sigma difference in the means and more safely quantify the evolution in the ULIRG velocity dispersion before and after nuclear coalescence.

The mean value of the rotational velocity is 56 $\mathrm{km\,s^{-1}}$ for the ULIRG remnants, increasing to 112 $\mathrm{km\,s^{-1}}$ when inclination effects are accounted for. The observed stellar rotational velocity of each individual source and its ratio over the dispersion is presented in Table 3. In Paper I we found that the progenitors have a $V_{\rm rot}/\ \sigma$ ratio of 0.42, which increases to 0.77 when correcting for inclination effects from the ellipticity of each individual progenitor. The mean $V_{\rm rot}$(obs)/σ ratio for the sample presented in this study is lower, 0.33, increasing to $V_{\rm rot}/\sigma$=0.66 when we apply a mean inclination correction to the rotational velocity. In this calculation we have not attempted to correct the central velocity dispersion for inclination effects.

The evolution of the velocity dispersion measured in ULIRGs is only a lower limit to the total dynamical heating that the interacting galaxies undergo during the merger. One of the reasons is that the ULIRG phase traces the merger periods during which strong starbursts occur; namely, beyond first encounter and close to nuclear coalescence (Mihos & Hernquist 1996; Mihos 1999; Springel et al. 2005; Veilleux et al. 2002). The starburst timescales are short ($\lesssim 10^8$ yrs; e.g. Canalizo & Stockton 2001) compared to that of the baryonic matter merging process (which lasts a few 10^9 yrs; e.g. Hernquist 1993). The fact that dynamical heating in the merging galaxies can be traced, even for these short timescales, is very significant.

Furthermore, even for the ultraluminous IR phases of a merger, any increase in σ that may possibly be observed is underestimated due to population effects. The host kinematics extracted from the NIR bandheads are often representative of those of young stellar populations i.e. giants and supergiants. These populations could still be linked to the gas from which they formed (which is believed to settle into a disk early compared to the stars in the progenitor disks: Mihos & Hernquist 1996), and have less perturbed orbits than the old stars. Therefore, host dispersions extracted from the CO bandheads may be systematically lower than those of the merging bulges. The low $V_{\rm rot}/\sigma$ ratio that we measure for our ULIRGs is a good indication that even the young stellar populations are significantly heated, and therefore, systematics originating from population effects are unlikely to have a

major effect on our conclusions.

It is possible that the sources used in this study and in Paper I originate from mergers of galaxies of somewhat different mass contents: the ULIRGs that are prior to nuclear coalescence may be more gas-rich (and possibly more massive) than the remnants in order to have an ultraluminous phase of comparable IR output at earlier merger phases (Mihos & Hernquist 1996). In that case, the observed dynamical heating may be less than what we would measure if we were able to observe a specific galaxy pair from the beginning until the end of the merging process. The molecular gas mass measurements obtained by Gao & Solomon (1999) in local Luminous Infrared Galaxies (LIRGs; sources of $10^{11} L_{\odot} < L_{\rm IR} < 10^{12} L_{\odot}$) and ULIRGs indicate that a correlation between nuclear separation and gas fraction is observed in LIRGs but not in ULIRGs. To properly investigate this possibility, an extended study of the molecular gas content of 1-Jy ULIRGs is now being performed (PI Tacconi).

4. Origin of the ULIRG remnants

We infer the initial conditions of the mergers that lead to ultraluminous IR activity by comparing the kinematic properties of ULIRG remnants with those predicted by simulations in the literature. According to various authors (e.g. Bendo & Barnes 2000; Naab & Burkert 2003) the remnant $V_{\rm rot}({\rm obs})/\sigma$ ratio is an indicator of the mass ratio of the merging galaxies. In the gas-free, N-body simulations of binary mergers performed by Naab & Burkert (2003) for several mass ratios and orientations, the major mergers produced slowly rotating remnants. Those authors suggested that the $V_{\rm rot}({\rm obs})/\sigma$ ratio is ~ 0.2 for 1:1 and ~ 0.4 for 2:1 merger remnants, while it reaches higher values (0.8) when the remnants originate from minor (4:1) mergers. Our remnants agree best with a 1:1 and 2:1 merger origin, also agreeing with the directly measured progenitor mass ratios of Paper I and confirming that ULIRGs are representative of the most violent local mergers.

Naab & Burkert (2003) and Burkert & Naab (2005) have also shown a connection between the $V_{\rm rot}({\rm obs})/\sigma$ ratio and the remnant ellipticity at the effective radius for several progenitor mass ratios. We overplot our results with those of Naab & Burkert (2003) in Fig. 3; our ULIRGs are given in stars, while the squares and the open diamonds correspond to boxy and disky isophotal-profile ellipticals (data provided to Naab & Burkert 2003 by R. Bender). Each panel corresponds to mergers of different progenitor mass ratios (denoted at the upper-left corner of each panel). Naab & Burkert (2003) show in bold, solid, and dotted contours the 90%,70%, and 50% probability of finding a merger remnant of each category in the enclosed region. These simulations did not include gas; the addition of gas would result in an increase of the remnant $V_{\rm rot}({\rm obs})/\sigma$ ratio (since the gas that is not consumed

during the merger will settle in a disk) and, therefore, to a shift of the probability contours to higher values on both axes (Burkert & Naab 2005). The position of our ULIRG remnants in this diagram gives further support to the argument that ULIRGs are produced mainly by mergers of galaxies of comparable masses (see Paper I).

5. End products of ultraluminous mergers

5.1. ULIRGs and the fundamental plane of early-type galaxies

The $V_{\rm rot}/\sigma$ ratio of the ULIRG remnants indicates that mergers of ultraluminous infrared output lead to dispersion-supported systems with a non-negligible rotational component (also see Genzel et al. 2001). To investigate what type of ellipticals ultraluminous IR mergers form, Genzel et al. (2001) and Tacconi et al. (2002) placed their sample of ULIRGs on the fundamental plane of early-type galaxies (Djorgovski & Davis 1987). They concluded that the remnants resemble moderate mass ellipticals (of stellar mass a few 10^{11} $M_{\odot}$). Our new data significantly increase the number of objects in the range of ULIRG luminosity to be compared with early-type galaxies.

The $R_{\rm eff}$ - σ projection of the plane that we construct from our data is shown in Fig. 4. Whenever possible, the K-band effective radius was used (Tacconi et al. 2002). Otherwise, we converted H- into K- band effective radii using an average correction derived from the $R_{\rm eff}$ values of Scoville et al. (2000) (for flux within 3 kpc). Data for early-type galaxies are taken from Bender et al. (1992), Faber et al. (1997), and Pahre (1999). Giant boxy ellipticals (squares) are located on the upper-right corner of the FP projection, while disky, moderate-mass ellipticals (circles) are at the center. ULIRGs, shown in triangles, agree very well with the location of the latter on the plane. Local LIRGs are mainly found at the lower-left corner of the FP projection (data from Shier & Fischer 1998 and James et al. 1999).

In Fig. 5 we show the 3-dimensional view of the fundamental plane, taking into account the central surface brightness of the sources. In the left panel, we use the K-band magnitudes from Kim et al. (2002); where total magnitudes (integrated up to the truncation radius) are not available, we use the magnitudes derived from the 4 kpc aperture photometry instead. We correct the magnitudes for extinction effects by subtracting 1.28 mag at 2.2 μm. We infer this (equivalent screen) correction from the study of Scoville et al. (2000) by converting the average 1.6 - 2.2 μm magnitude difference of their sample (0.84 for 2 kpc aperture photometry) into color excess. We then compute the mean surface brightness within the effective radius $< \mu_{\rm eff} >$ of each source by adding $2.5log(2\pi R_{\rm eff}^2)$ mags (where $R_{\rm eff}$ is in $''$) to

its extinction-corrected magnitude.

High-resolution NIR imaging of 22 ULIRG remnants has recently been performed by Veilleux et al. (2006) using the Hubble Space Telescope NICMOS camera. For these images, point spread function (PSF) subtraction has been performed to separate AGN and host galaxy light. Since nuclear starburst emission also contributes to the central PSF (in addition to the AGN continuum), the computed host magnitudes are upper limits to the actual values. For the sources in our sample that have been observed with NICMOS, we derive the host H-band magnitudes from their absolute values $M_{\rm host}$ presented in Veilleux et al. (2006) and convert them into K-band magnitudes using the average correction from Scoville et al. (2000). For the remaining sources, we derive the host ($M_{\rm host}$) from the total absolute magnitudes ($M_{\rm tot}$) by applying the mean $M_{\rm host} - M_{\rm tot}$ difference of the Veilleux et al. (2006) sample (1.19 mag) to the K-band photometric results of Kim et al. (2002). For our pre-coalescence sources, the strength of the subtracted PSF is probably higher than in reality because the ULIRG sample of Veilleux et al. (2006) consists mainly of coalesced sources. After applying an extinction correction identical to that of Fig. 5 (left panel) to the host magnitudes and calculating $< \mu_{\rm eff} >$, we present the NICMOS-data based view of the FP in Fig. 5 (right panel).

In the 3-dimensional view of the plane, ULIRGs tend to deviate from the position of early-type galaxies (along the surface brightness axis). This is due to extinction and population effects (Tacconi et al. 2002). Due to the strong starbursts in ULIRGs, they have a significant population of asymptotic-giant-brach stars, red giants and supergiants. Thus, their NIR surface brightnesses are higher than those of quiescent ellipticals.

5.2. The masses of ultraluminous merger remnants

A direct way to verify that ULIRGs form moderate-mass ellipticals is to calculate the mass m of the remnants, which according to Bender et al. (1992) is related to the stellar kinematics as $m = c_2 \sigma_{100}^2 R_{\rm eff}$, where σ_{100} is the projected central velocity dispersion in units of 100 $\rm km\,s^{-1}$, $R_{\rm eff}$ is in kpc, and m is in 10^{10} $M_\odot$. The geometrical factor c_2 depends on the distribution of matter in the galaxy. Following Tacconi et al. (2002), we adopt $c_2 = 1.4$, as appropriate for a constant m/L King model whose tidal-to-core radius ratio is 50, midway between those of dwarf and giant ellipticals. By combining the above, the dynamical mass enclosed within two half-light radii is computed from $m = 4.7 \times 10^5 (3\sigma^2 + {V_{\rm rot}}^2) R_{\rm eff}$, where σ and $V_{\rm rot}$ are now in units of $\rm km\,s^{-1}$ and m is in $M_\odot$.

We use the mean values of the stellar dispersion and inclination-corrected rotational

velocity from § 3. Whenever $V_{\rm rot}$ is not available, we use the mean inclination-corrected $V_{\rm rot}/\sigma$ ratio to infer it. We find that the mean dynamical mass of the remnants is 8.86×10^{10} $M_{\odot}$ (in good adreement with Tacconi et al. 2002), suggesting that ultraluminous activity mainly originates from mergers of sub-m_* galaxies, for $m_* = 1.4 \times 10^{11}$ $M_{\odot}$ (Genzel et al. 2001 and references therein). For different values of m_* (e.g that of Bell et al. 2003 adapted to our cosmology, 8.3×10^{10} $M_{\odot}$) the sub-m_* characterization of ULIRGs may change to $\sim m_*$. Still, in the local Universe, the galaxies that when merging can be observed as ULIRGs do not need to be as massive as e.g. the Milky Way.

This conclusion does not contradict the result of Veilleux et al. (2006) that the H-band host magnitude $M(H)$ of the ULIRGs they studied is, on average, greater than $1.5M_*(H)$, for $M_*(H) = -23.7$. Because of the strong starbursts ULIRGs undergo, their luminosity-to-mass ratio does not remain constant throughout the merger process (see also Tacconi et al. 2002; Rupke et al. 2002; 2005a; 2005b).

ULIRG masses derived from Hα emission-line dispersions are also sub-m$_*$ (Colina et al. 2005). Tracing the ionized gas by the [FeII] emission lines that appear in our spectra, we find that while the mean dispersion of the gas is similar to that of the stars, in individual cases gas and stellar dispersions may significantly deviate due to gas outflows. Gas kinematics in these ULIRGs will be presented in a forthcoming paper (Tacconi et al. 2006, in preparation).

5.3. Can ULIRGs form giant Es?

Our main conclusion is that ULIRGs form elliptical galaxies of significantly lower mass than that of giant ellipticals (of typical stellar mass $\gtrsim 5\times10^{11}$ $M_{\odot}$). It is therefore reasonable to investigate whether local ULIRGs could also form few giant ellipticals or whether the size of the current sample is not large enough to permit a definite answer.

For this assessment, we used the mass function of local Es to estimate what fraction f of the sources with mass $> 10^{10}\,M_{\odot}$ (mass threshold similar to that of ULIRGs) corresponds to giant ellipticals (of stellar mass $> 5 \times 10^{11}\,M_{\odot}$). Given that the fraction may significantly vary according to the adopted mass function, we used the best fit to the K-band mass function from various authors in the literature. Giant ellipticals comprise 18.7% of local Es with mass $> 10^{10}\,M_{\odot}$ for the mass function of Bell et al. (2003), found for Es in the Sloan Digital Sky (SDSS) and the Two Micron All Sky (2MASS) surveys for a diet[2] Salpeter initial mass function (IMF). The fraction f is 20.1% for the 2MASS K-band luminosity function

[2]of stellar mass reduced by 30%

of local Es (Kochanek et al. 2001) which we convert to mass function using $m/L = 1.32$ $M_{\odot}/L_{\odot}$ (Cole et al. 2001). This K-band m/L ratio is computed for both early- and late-type galaxies in the 2MASS and 2dF Galaxy Redshift Surveys, assuming a Salpeter IMF. An estimate of the m/L ratio for local ellipticals only can be derived from the work of Cappellari et al. (2005a) using the mean I-band m/L value and I-K color correction of the SAURON project sources. Combining the 2MASS K-band luminosity function with this early-type-galaxy m/L value (0.75 $M_{\odot}/L_{\odot}$) yields f=10.9%. Although f is between 10% and 20%, we do not observe any source of $m > 5 \times 10^{11}$ $M_{\odot}$ in our sample of 30 ULIRG remnants; this fact indicates that the formation of few giant ellipticals cannot be considered typical for local ultraluminous mergers, though it cannot be excluded by our statistics.

In Fig. 6, we compare the number density of ULIRG remnants and ellipticals as a function of their stellar dispersion (in the range between 50 and 300 $\mathrm{km\,s^{-1}}$). The source number density per stellar dispersion, $n(\sigma)$, is shown as a histogram for ULIRGs and as a solid line for SDSS ellipticals. For the ellipticals, $n(\sigma)$ is computed from the velocity dispersion function of Sheth et al. (2003). The $n(\sigma)$ distribution of local ULIRGs is calculated by multiplying the % fraction of ULIRG remnants per σ bin with the (converted to our cosmology) volume density of ULIRGs (2.5×10^{-7} $\mathrm{Mpc^{-3}}$) from Sanders et al. (2003). To facilitate the comparison between the two $n(\sigma)$ distributions, we apply a normalization factor of 7×10^3 to the ULIRG histogram so that its mean has the same number density as that of the SDSS ellipticals. Physically, this normalization factor is related to the ratio between the time over which ellipticals have been formed and the lifetime of a single ultraluminous burst. Its value is only a rough estimate since it depends on the completeness of the 1 Jy and the SDSS (sub-)samples and the fact that ultraluminous mergers are not the only mechanism to produce elliptical galaxies.

A Gaussian fit to the elliptical-galaxy $n(\sigma)$ distribution leads to a mean dispersion identical to that of ULIRGs, 157 ($\pm$54) $\mathrm{km\,s^{-1}}$. In other words, the descendants of ULIRGs will resemble the ellipticals that are most common in the local Universe. Local ULIRGs seem to form at highest rates sources of characteristic σ between 130 and 160 $\mathrm{km\,s^{-1}}$.

At high and low dispersions, the ratio between $n(\sigma)$ and $n(<\sigma>)$ seems to be lower for ULIRGs than for ellipticals. The deviations between the two distributions at the low-dispersion end may be due to the fact that mergers of gas-rich galaxies below a certain mass threshold do not possess enough gas to undergo a ULIRG phase. For the high-dispersion end, we cannot formally rule out the possibility that some ULIRGs may have been missed either due to sample incompleteness or to possible shorter (than the average) burst timescales of the most massive sources. However, a more possible scenario can be derived from the work of Thomas et al. (2005); namely that the more massive galaxies are, the faster and the earlier

their stellar population have formed. Another plausible explanation is that at low redshifts other types of mergers (e.g. elliptical-spiral or elliptical-elliptical ones) may significantly account for the formation of giant Es (Khochfar & Burkert 2003).

5.4. Wavelength dependence of the stellar velocity dispersion measurement

Systematic differences between the measured and the actual values of the host dispersion can arise when extracting σ from different wavelengths, i.e. from the Ca II triplet in the optical (e.g. Rothberg & Joseph 2005) and the CO bandheads in the NIR. When using CO, the systematics originate from population effects (see § 3), while in the case of the Ca triplet, the systematics are mainly related to the presence of dust. Due to scattering of light from dust particles, photons originating from high-velocity stars in the center of the galaxy will be scattered into random lines of sight. This will particularly bias the LOS velocity distribution at large radii where host dispersion is lower than that in the center (Baes & Dejonghe 2002). The effects of dust in the observed stellar kinematics will further increase with increasing dust mass and extent (Baes & Dejonghe 2002). Since ULIRGs are highly obscured systems, dispersions extracted from the Ca triplet may be systematically higher than those of the stars in the central spheroid.

Silge & Gebhardt (2003) have attempted to quantify the (possible) discrepancy between dispersion estimates derived from the NIR and the optical regimes for local quiescent galaxies. While they found no significant difference for elliptical galaxies, the systematics were non-negligible in S0 lenticulars, with the largest difference in σ ($\sim$30-40%) found in the most massive sources of their sample. Typical $V_{\rm rot}/\sigma$ ratios for S0 lenticulars are greater than those of ULIRGs, $\gtrsim 1.5$ (e.g., Pizzela et al. 2005; Cappellari et al. 2005b) indicating that deviations of the order 30-40% between the CO and Ca dispersion measurement are probably high for ULIRGs.

To investigate how using the Ca II triplet for the measurement of σ might affect the results of this paper, we increase our sample's average dispersion by 40% (the maximum reported deviation between the NIR and the optical results in Silge & Gebhardt 2003). This increase corresponds to 60 $\rm km\,s^{-1}$ or a shift of 0.15 in logarithmic space, bringing merger remnants closer to (but not within) the FP region populated by giant ellipticals. When applying this maximum correction of 60 $\rm km\,s^{-1}$ to the dispersion of the binary ULIRGs, we find that the masses of the progenitors would still be close to m_* (1.66×10^{11} $M_\odot$, on average).

Rothberg & Joseph (2005), who measured σ from Ca triplet optical spectroscopy for

13 LIRG and 3 ULIRG remnants, found that the hypothesis that luminous/ultraluminous mergers and giant ellipticals are drawn from the same parent population can be rejected at confidence levels of 0.1. This is, again, an indication that ULIRGs may be able to form few giant ellipticals.

6. A picture of the $M_{\rm BH}$-σ relation time evolution

The size of a black hole seems to be closely linked to the depth of the potential well in which it forms and grows (Ferrarese & Merritt 2000). This is reflected i.e. in the local $M_{\rm BH} - \sigma$ relation, the correlation between $M_{\rm BH}$ and the stellar dispersion in the bulge of the host galaxy (Ferrarese & Merritt 2000; Gebhardt et al. 2000). Since the $M_{\rm BH} - \sigma$ relation is found for (virialized) bulge systems, it should be valid at the end of the merger process, when the bulge stellar kinematics have reached their final dynamical state and AGN winds and supernovae feedback have expelled the gas away from the nucleus, preventing further BH growth, terminating the starburst phase, and making the system resemble an elliptical galaxy. The merger remnants in the simulations of Di Matteo et al. (2005) and Springel et al. (2005) are able to reproduce the $M_{\rm BH} - \sigma$ relation by subjecting a portion of their interstellar gas to accretion and feedback.

For ULIRGs however, the conversion of the host velocity dispersion into $M_{\rm BH}$ carries the uncertainty of applying the $M_{\rm BH} - \sigma$ relation to systems out of dynamical equilibrium. It is not yet known if, or to what extent, the $M_{\rm BH} - \sigma$ relation is valid between the first encounter and shortly ($\lesssim 10^8$ yrs) after the final coalescence, when most of the ultraluminous infrared activity occurs.

To investigate whether merging disk galaxies fall on the $M_{\rm BH} - \sigma$ relation during some interaction phases, we ran gas-rich merger simulations (details to be presented in Naab et al. 2006, in preparation) that have already been discussed briefly in Paper I. To include the effects of a dissipative component we replaced 10% of the stellar mass in the initial disks with isothermal gas at a temperature of approximately 10000K. The initial scale length of the gas disk was equal to that of the stellar disk, h. Each galaxy had a stellar bulge with 1/3 of the disk mass and was embedded in a pseudo-isothermal halo to guarantee a flat rotation curve at large radii. All galaxies approached each other on nearly parabolic orbits with a pericenter distance of two disk scale lengths. The evolution of the stars and the gas was computed with the N-body smoothed-particle-hydrodynamics code VINE using an isothermal equation of state for the gas. For this study we analyzed mergers with 16 different initial disk orientations (geometries 1-16 of Naab & Burkert 2003) and mass ratios 1:1 and 3:1.

We analyzed snapshots in the orbital plane approximately every half-mass rotation period of the more massive disk to follow the time evolution of the (projected) central stellar velocity dispersion and the gas accretion history onto the center of the system. At each snapshot, we calculated $M_{\rm BH}$ from the velocity dispersion assuming that the $M_{\rm BH}-\sigma$ relation is always valid. As in Paper I, we used the Tremaine et al. (2002) formula $M_{BH}=1.35\times10^{8}[\sigma/200]^{4.02}\,M_{\odot}$, where σ is in units of $\rm km\,s^{-1}$, to calculate the black hole masses. To quantify the gas accretion, we computed the total gas mass $M_{\rm gas}$ that has ever reached a radius of $0.1h$ (i.e. twice the resolution element of the simulations) around the mass center of the system. By calculating the ratio between the quantities $M_{\rm BH}$ and $M_{\rm gas}$ we derive the accretion efficiency ϵ that is needed to maintain the black hole mass on the Tremaine et al. (2002) formula at any time. We define accretion efficiency ϵ as the fraction of the gas that accretes onto the black hole from the gas accumulated into the nuclear region.

In Fig. 7 we show the evolution of the accretion efficiency (needed to keep the black hole on the $M_{\rm BH}-\sigma$ relation) as a function of time (left column) and nuclear separation (right column). The efficiency is averaged over the 16 initial geometries for 1:1 and 3:1 mergers (upper and lower panels). The diagonally shaded area indicates the spread due to the varying initial disk geometries.

According to the left panels of Fig. 7, before nuclear coalescence, the estimated black hole mass and the gas accumulated at the center of the simulation already scale linearly. In other words, if we assume that the $M_{\rm BH}-\sigma$ relation is valid at *any* time during the merger, then the accretion efficiency remains constant shortly after the first encounter (shown in vertical dashes) until relaxation. Vice-versa, if we assume that the $M_{\rm BH}-\sigma$ relation is *only* valid at relaxation and that ϵ stays constant during the merger, then the black hole mass can be computed from the $M_{\rm BH}-\sigma$ relation until close to first encounter (backwards in time). Assuming that the $M_{\rm BH}-\sigma$ relation is valid at relaxation is reasonable since the remnants are young elliptical galaxies.

In the right panels of Fig. 7, the "folding" of the efficiency ϵ at large nuclear separations is due to the fact that the galaxies move towards apogalacticon before they fall back together. Clearly, at these merger phases, the use of the $M_{\rm BH}-\sigma$ relation can be misleading. For a constant ϵ, the $M_{\rm BH}-\sigma$ relation begins to be valid beyond 5 disk scale lengths, which corresponds to a nuclear separation $\sim$7 kpc for our ULIRGs (see Paper I). If the assumption of a constant ϵ holds, the black hole estimates for $\sim 2/3$ of the binary sources may be considered realistic (but still lower limits on their actual values). For the ULIRG remnants, computing BH masses from stellar dispersions seems also plausible. This is further supported by the fact that the kinematics of the latter are expected to have almost settled to their relaxation values (Mihos 2000). We acknowledge, however, that the efficiency ϵ may drastically vary during

accretion events; therefore all black hole estimates calculated from the $M_{\rm BH} - \sigma$ relation are carrying this uncertainty.

7. Discussion on the black hole mass evolution

We calculate the individual black hole masses of the sources in our sample using the Tremaine et al. (2002) formula and tabulate the results in Table 3. Since our sources are still in an ultraluminous IR emission phase, gas and dust are still present in the nuclear region and will continue accreting onto the black hole. However, beyond coalescence, the timescales for further gas accretion onto the black hole are probably shorter than those of the pre-coalescence stabursts (e.g. Springel et al. 2005). Therefore, the black hole masses of the fully relaxed systems will be somewhat larger than those presented in Table 3. Simple gas content (typical gas mass of ULIRGs is 5×10^9 $M_\odot$; Downes & Solomon 1998) and accretion efficiency (0.01, see § 6) arguments indicate that the additional increase of the remnant BH masses will not exceed 10^8 $M_\odot$ by the time the ultraluminous activity ends. In this order-of-magnitude calculation we have ignored the fact that only part of the gas reaches (or remains in) the center of the merging system, further reducing the upper limit on the black hole mass.

We calculate the BH mass each source would have, if it were accreting at the Eddington rate ($L_{\rm Edd}/L_\odot = 3.8 \times 10^4 M_{\rm Edd}/M_\odot$). To calculate the Eddington BH mass $M_{\rm Edd}$, we assign to the Eddington luminosity $L_{\rm Edd}$ half of the luminosity emitted in the IR (Genzel et al. 1998; Sanders & Mirabel 1996), given that some ULIRGs are largely starburst- while others are AGN- powered. The Eddington efficiency $\eta_{\rm Edd}$, the ratio of the Eddington over the dynamical black hole mass, is given in Table 3. The mean Eddington efficiency of the merged-ULIRG sample is 0.93, with a wide spread of values. While statistically appropriate, the assumption that 50% of the IR luminosity originates from the AGN may make some sources appear as if accreting at super-Eddington rates (see Table 3). If we assign $\eta_{\rm Edd}$=1 for these sources and recalculate the average efficiency, we find it to be 0.51.

The inferred accretion rates may be higher than in reality if an overestimated fraction of the IR emission is assigned to the AGN. This could occur, if for example, the starburst is still the dominant source of the IR luminosity after the merging nuclei coalesce. The relative strengths of the starburst ($L_{\rm SB}$) and the AGN ($L_{\rm AGN}$) luminosity at each merger phase are uncertain. However, the MIR ISO spectroscopic study of local ULIRGs by Genzel et al. (1998) and Rigopoulou et al. (1999) indicates that most ULIRGs are starburst dominated systems, implying that probably less than 50% of the IR luminosity should be assigned to the AGN. Furthermore, simulations predict that strong starburst episodes precede high

accretion-rate phases (see Mihos & Hernquist 1996, Springel et al. 2005, Di Matteo et al. 2005). Observations (Veilleux et al. 2002) indicate that the strength of nuclear (continuum) emission increases with decreasing nuclear separation. Therefore, the Eddington efficiencies of the progenitors presented in Paper I may be systematically overestimated compared to those of the remnants. Future papers presenting SPITZER MIR spectroscopy of local ULIRGs will indicate the appropriate luminosity fraction that needs to be assigned to the AGN for ULIRGs before and after nuclear separation.

8. Conclusions

We have acquired spectroscopic H-band, long-slit, data of 54 ULIRGs at a variety of merger phases to trace the evolution of their host dynamical properties. We find that:

1. Indications of an increase of the stellar random motions exist as the merger advances. The mean stellar σ, as measured from the CO rovibrational bandheads, equals 143 $\mathrm{km\,s^{-1}}$ for the binary sources (of mean nuclear separation 8.0 kpc, including IRAS 00456-2904) and 157 $\mathrm{km\,s^{-1}}$ for the remnants. This difference in the means of the pre- and post- coalescence distributions is marginally significant and requires more data to be accurately constrained. Furthermore, any increase of the stellar dispersion observed in ULIRGs corresponds to only a part of the dynamical heating that occurs during the merger, since the merger timescales are longer than those of the ultraluminous starburst.

2. The dynamical and structural properties of the remnants indicate that they originate from mergers mainly of 1:1 and 2:1 progenitor mass ratios. This confirms what we found in Paper I by directly measuring the masses of the individual progenitors of binary ULIRGs.

3. Ultraluminous mergers will mainly lead to the formation of moderate mass ellipticals (of stellar mass $\sim 10^{11}\,M_{\odot}$). Depending on the definition of m_*, ULIRGs are between sub- and $\sim m_*$. ULIRGs are located in a region of the fundamental plane of early-type galaxies different from that of local giant Es, possibly indicating a different formation history for the latter. Local mass and dispersion functions support this argument; however, the current statistics cannot exclude the formation of few giant Es from ULIRGs.

4. We have performed simulations to investigate whether a black hole mass-host dispersion relation may be used to calculate the black hole masses of our ULIRGs. We find that

already before nuclear coalescence, the mass of the gas that falls into the center of the merging system scales linearly with the black hole mass predicted by the $M_{\rm BH} - \sigma$ relation. However, this is only true if the efficiency of gas accretion onto the BH from its surroundings remains constant with time.

5. The black hole masses of the merged ULIRGs are of the order 10^7-$10^8\,M_\odot$ and their accretion rates are high (Eddington efficiencies often > 0.5). If the AGN luminosity output of a ULIRG nucleus increases with time, our accretion rates in pre-coalescence ULIRGs may be overestimated relative to post-coalescence ULIRGs.

We are grateful to N. Scoville for providing us H-band NICMOS imaging data for two of our sources and D. C. Kim for frequently giving us prior-to-publication NICMOS photometric results for several sources. We would like to thank the ESO VLT staff for their support both in the service and visitor mode data acquisition. A. J. Baker acknowledges support from the National Radio Astronomy Observatory, which is operated by Associated Universities, Inc., under cooperative agreement with the National Science Foundation.

REFERENCES

Baes, M. & Dejonghe, H. 2002, MNRAS, 335, 441

Bell, E. F., McIntosh, D. H., Katz, N., Weinberg, M. D. 2003, ApJS, 149, 289

Bender, R. 1990, A&A, 229, 441

Bender, R., Burstein, D., & Faber, S. M. 1992, ApJ, 399, 462

Bendo, G. J., & Barnes, J. E. 2000, MNRAS, 316, 315

Bertin, E., & Arnouts, S. 1996, A&AS, 117, 393

Binney J., & Tremaine S. 1987, Galactic Dynamics, Princeton Univ. Press.

Bryant, P. M., & Scoville, N. Z. 1999, AJ, 117, 2632

Burkert, A. & Naab, T. 2005, MNRAS, 363, 597

Canalizo, G., & Stockton, A. 2001, ApJ, 555, 719

Cappellari, M., et al. 2005, in press, astro-ph/0505042

Cappellari, M., et al. 2005, in press, astro-ph/0509470

Cole, S., et al. 2001, MNRAS, 326, 255

Colina, L., Arribas, S., Monreal-Ibero, A. 2005, ApJ, 621, 725

Dasyra, K. M., Tacconi, L. J., Davies, R.I., Lutz, D., Genzel, R., Burkert, A., Veilleux, S. & Sanders, D. 2005, ApJ, in press (astro-ph/0510670)

Di Matteo, T., Springel, V., & Hernquist, L. 2005, Nature, 433, 604

Djorgovski, S., & Davis, M. 1987, ApJ, 313, 59

Duc P.-A., Mirabel, I.F., & Maza, J. 1997, A&AS, 124, 533

Downes, D., & Solomon, P.M. 1998, ApJ, 507, 615

Dressler, A., Lynden-Bell, D., Burstein, D., Davies, R. L., Faber, S. M., Terlevich, R., & Wegner, G. 1987, ApJ, 313, 42

Dunlop, J. S, McLure, R. J., Kukula, M. J., Baum, S. A., O'Dea, C. P., & Hughes, D. H. 2003, MNRAS, 340, 1095

Faber, S. M., et al. 1997, AJ, 114, 1771

Ferrarese, L., & Merritt, D. 2000, ApJ, 539, L9

Gao, Y., & Solomon, P. M. 1999, ApJ, 512, L99

Gebhardt, K. et al. 2000, ApJ, 543, L5

Genzel, R., Lutz, D., Sturm, E., Egami, E., Kunze, D., Moorwood, A. F. M., Rigopoulou, D., Spoon, H. W. W., Sternberg, A., Tacconi-Garman, L. E., Tacconi, L., & Thatte, N. 1998, ApJ, 498, 579

Genzel, R., Tacconi, L. J., Rigopoulou, D., Lutz, D., & Tecza, M. 2001, ApJ, 563, 527

Hernquist, L. 1993, ApJ, 409, 548

James, P., Bate, C., Wells, M., Wright, G., & Doyon, R. 1999, MNRAS, 309, 585

Kauffmann, G.; White, S. D. M. 1993, MNRAS, 261, 921

Khochfar, S., Burkert, A. 2003ApJ, 597L, 117

Kim, D.-C., Veilleux, S., & Sanders, D. B. 2002, ApJS, 143, 277

Kochanek, C. S., et al. 2001, ApJ, 560, 566

Kormendy, J., Sanders, D. B. 1992, ApJ, 390L, 53

Le Fèvre, O., et al. 2000, MNRAS, 311, 565

Lutz, D., Veilleux, S., & Genzel, R. 1999, ApJ, 517L, 13

Mihos, J. C., & Hernquist, L. 1996, ApJ, 464, 641

Mihos, J. C. 1999, Ap&SS, 266, 195

Mihos, J. C. 2000, ASPC, 197, 275

Moorwood, A. F. M., et al. 1998, Messenger, 94, 7

Naab, T., & Burkert, A. 2003, ApJ, 597, 893

Pahre, M. A. 1999, ApJS, 124, 127

Pizzella, A., Corsini, E. M., Dalla Bonta, E., Sarzi, M., Coccato, L., Bertola, F. 2005, ApJ, 631, 785

Rigopoulou, D., Spoon, H. W. W., Genzel, R., Lutz, D., Moorwood, A. F. M., & Tran, Q. D. 1999, AJ, 118, 2625

Rothberg, B., & Joseph, R. D. 2005, astro-ph/0510019

Rupke, D. S., Veilleux, S., & Sanders, D. B. 2002, ApJ, 570, 588

Rupke, D. S., Veilleux, S., & Sanders, D. B. 2005, ApJS, 160, 115

Rupke, D. S., Veilleux, S., & Sanders, D. B. 2005, ApJ, 632, 751

Sanders, D. B., & Mirabel, I. F. 1996, ARA&A,34,749

Sanders, D. B., Mazzarella, J. M., Kim, D.-C., Surace, J. A., Soifer, B. T. 2003 AJ, 126, 1607

Schmidt, M. & Green, R. 1983, ApJ, 269, 352

Scoville, N. Z., Evans, A. S., Thompson, R., Rieke, M., Hines, D. C., Low, F. J., Dinshaw, N., Surace, J. A., & Armus, L. 2000 AJ, 119, 991

Sheth, R. K., et al. (2003), ApJ, 594, 225

Shier, L. M., & Fischer, J. 1998, ApJ, 497,163

Silge, J., & Gebhardt, K. 2003, AJ, 125, 2809

Springel, V., Di Matteo, T., & Hernquist, L. 2005, MNRAS, 361, 776

Tacconi, L. J., Genzel, R., Lutz, D., Rigopoulou, D., Baker, A. J., Iserlohe, C., & Tecza, M. 2002, ApJ, 580, 73

Tecza, M., Genzel, R., Tacconi, L. J., Anders, S., Tacconi-Garman, L. E., & Thatte, N. 2000, ApJ, 537, 178

Thomas, D., Maraston, C., Bender, R., de Oliveira, C. M. 2005, ApJ, 621, 673

Tremaine, S., Gebhardt, K., Bender, R., Bower, G., Dressler, A., Faber, S. M., Filippenko, A. V., Green, R., Grillmair, C., Ho, L. C., Kormendy, J., Lauer, T. R., Maggorian, J., Pinkney, J., & Richstone, D. 2002 ApJ, 574, 740

Veilleux, S., Kim, D.-C., & Sanders, D. B. 2002, ApJS, 143, 315

Veilleux, S., et al. 2006, ApJ, submitted

Table 1. List of ULIRG remnants

Galaxy (IRAS)	RA (2000)	Dec (2000)	z	$\log(L_{\rm IR}/{\rm L}_\odot)$	slit P.A. (°)	$t_{\rm integration}$ (mins)
00091−0738	00:11:43.3	−07:22:08	0.118	12.19	17,106	60,60
00262+4251 [a]	00:28:54.0	+43:08:18	0.0927	12.02	45,0	20,60
00397−1312	00:42:15.5	−12:56:04	0.262	12.90	-1,89	120,120
00456−2904 [a,b]	00:48:06.8	−28:48:19	0.110	12.12	30	40
01004−2237	01:02:49.9	−22:21:57	0.118	12.24	-1,89	60,60
01388−4618 [a]	01:40:55.9	−46:02:53	0.090	12.03	0,90	40,40
01572+0009 (Mrk 1014) [a]	01:59:50.2	+00:23:41	0.163	12.53	20, -70	80, 60
02021−2103	02:04:27.3	−20:49:41	0.116	12.01	53,142	60,60
04103−2838	04:12:19.5	−28:30:24	0.117	12.55	89	60
04313−1649	04:33:37.1	−16:43:32	0.268	12.55	-1,89	120,120
05189−2524	05:21:01	−25:21:46	0.043	12.09	-1,89	200,160
09039+0503	09:06:34.2	+04:51:25	0.125	12.07	-1,89	60,60
09111−1007	09:13:38.8	−10:19:20	0.054	11.95	34,124	120,60
11223−1244	11:24:50	−13:01:13	0.199	12.59	-1,89	80,80
12540+5708 (Mrk 231) [a]	12:56:14.2	−56:52:25	0.042	12.50	10,-30,-80	40,40,40
13428+5608 (Mrk 273) [a]	13:44:42.1	−55:53:13	0.037	12.13	15,95	40,40
14070+0525	14:09:31.3	+05:11:31	0.264	12.76	-1,89	120,120
14378−3651 [a]	14:40:58.9	−37:04:33	0.068	12.24	-45	80
15130−1958	15:15:55.2	−20:09:17	0.109	12.09	-171,-81	80,110
15250+3609 [a]	15:26:59.4	−35:58:38	0.055	11.99	45, -45	40,40
15462−0450	15:48:56.8	−04:59:34	0.100	12.16	179,-91	180,160
17208−0014 [a]	17:23:21.9	−00:17:00	0.0428	12.33	90,120	30, 30
20087−0308 [a]	20:11:23.2	−02:59:54	0.106	12.40	-45,45	40,40
20414−1651	20:44:18.2	−16:40:16	0.087	12.26	54,144	100,80
20551−4250 [a]	20:58:26.9	−42:39:06	0.0428	11.98	-45,45	60,60
21219−1757	21:24:41.6	−17:44:46	0.112	12.06	-1,89	50,40
21504−0628	21:53:05.5	−06:14:50	0.078	11.92	-39,59	60,60
23230−6926	23:26:03.6	−69:10:19	0.106	12.17	-1,89	60,60
23365+3604 [a]	23:39:01.3	+36:21:10	0.0645	12.09	45, -30	15, 40
23578−5307 [a]	00:00:23.6	−52:50:28	0.125	12.10	107,14	60, 40

Note. — The coordinates, the redshift, the bolometric luminosity, as well as the position angles and respective integration time for our sources are presented in this Table.

[a]Sources presented in Genzel et al. (2001) and Tacconi et al. (2002).

[b]According to the imaging analysis of Kim et al. (2002) and Veilleux et al. (2006) this source probably is a binary system at projected nuclear separation of 20.7 kpc. The redshift of the NE nucleus is not spectroscopically confirmed but its ambiguous morphology indicates an interaction. The data presented in this paper are for the more luminous (late-type-host) SW nucleus.

Table 2. ULIRG structural parameters

Galaxy (IRAS)	$R_{\rm eff}(H\ band)$ (kpc)	ellipticity	ϕ_α (°)
00091−0738 [a]	2.47(±0.21)	0.220	15
00262+4251 [b]	...	...	...
00397−1312 [c]	2.04 (±0.76)	0.35	-25
00456−2901 [a]	2.09 (±0.15)	0.067	-88
01004−2237 [c]	0.40 (±0.07)	0.02	26
01388−4618 [a]	1.62 (±0.03)	0.074	55
01572+0009 [a]	1.31 (±0.10)	0.140	81
02021−2103 [c]	5.38 (±3.95)	0.34	1
04103−2838 [c]	1.61 (±0.12)	0.19	-80
04313−1649 [c]	4.04 (±0.89)	0.26	86
05189−2524 [c]	0.57 (±0.08)	0.06	77
09039+0503 [c]	1.62 (±0.90)	0.15	-18
09111−1007 [a]	2.18 (±0.36)	0.397	-26
11223−1244 [a]	3.83 (±0.38)	0.101	70
12540+5708 [c]	1.40 (±0.21)	0.08	-11
13428+5608 [d]	1.03 (±1.03)	0.498	-77
14070+0525 [c]	3.62 (±0.53)	0.17	-19
14378−3651 [a]	0.36 (±0.02)	0.031	20
15130−1958 [c]	1.62 (±0.27)	0.23	-88
15250+3609 [d]	1.10 (±0.09)	0.207	-72
15462−0450 [c]	5.57 (±1.38)	0.048	62
17208−0014 [a]	1.69 (±0.08)	0.196	54
20087−0308 [a]	1.87 (±0.22)	0.324	-86
20414−1651 [c]	1.37 (±0.47)	0.67	3
20551−4250 [a]	1.32 (±0.25)	0.113	84
21219−1757 [c]	4.19 (±3.29)	0.14	-50
21504−0628 [a]	1.95 (±0.26)	0.164	12
23230−6926 [a]	2.03 (±0.25)	0.177	41
23365+3604 [b]	...	...	...
23578−5307 [a]	3.96 (±1.36)	0.447	-80

[a]The ULIRG structural parameters derived from the H-band acquisition images.

[b]For the sources observed using NIRSPEC and the slit monitoring camera, the structural parameters are not extracted; the slit projection drawn on the acquisition image does not allow for photometric analysis.

[c]Data taken from H-band NICMOS imaging by Veilleux et al. (2006, submitted). Effective radii are converted to our cosmology.

[d]Parameters extracted from NICMOS imaging data (at 1.6 μm), kindly provided to us by Nick Scoville (see Scoville et al. 2000).

Table 3. Stellar velocities and resulting black hole masses

Source (IRAS)	σ (km s^{-1})	$V_{\rm rot}$(obs) [a] (km s^{-1})	$V_{\rm rot}$(obs)/σ	$M_{\rm BH}$ [b] ($M_\odot$)	$M_{\rm BH}$(Edd.) [c] ($M_\odot$)	$\eta_{\rm Edd}$ [d]
00091−0738	131 (± 39)	···	···	2.46×10^7	2.04×10^7	0.83
00262+4251 [e]	170 (± 15)	···	···	7.02×10^7	1.32×10^7	0.19
00397−1312	106 (± 26)	49 (± 17)	0.46	1.05×10^7	1.05×10^8	9.94
00456−2901	162 (± 25)	45 (± 10)	0.28	5.79×10^7	1.73×10^7	0.30
01004−2237	132 (± 29)	22 (± 13)	0.17	2.54×10^7	2.29×10^7	0.90
01388−4618	144 (± 10)	130 (± 15)	0.90	3.60×10^7	1.32×10^7	0.37
01572+0009	200 (± 60)	···	···	1.35×10^8	4.46×10^7	0.33
02021−2103	143 (± 21)	42 (± 10)	0.29	3.50×10^7	1.35×10^7	0.38
04103−2838	129 (± 40)	4 (± 5)	0.03	2.32×10^7	1.86×10^7	0.80
04313−1649	157 (± 21)	31 (± 27)	0.20	5.10×10^7	4.67×10^7	0.92
05189−2524	137 (± 16)	70 (± 14)	0.51	2.95×10^7	1.62×10^7	0.55
09039+0503	183 (± 38)	···	···	9.45×10^7	1.55×10^7	0.16
09111−1007	112 (± 18)	68 (± 16)	0.61	1.31×10^7	9.53×10^6	0.73
11223−1244	149 (± 27)	···	···	4.13×10^7	5.12×10^7	1.24
12540+5708	120 (± 10)	25 (±10)	0.21	1.73×10^7	4.16×10^7	2.40
13428+5608	285 (± 30)	110 (±20)	0.39	5.61×10^8	1.66×10^7	0.03
14070+0525	139 (± 21)	54 (± 19)	0.39	3.13×10^7	7.57×10^7	2.42
14378−3651	153 (± 10)	15 (±10)	0.10	4.60×10^7	1.66×10^7	0.36
15130−1958	177 (± 39)	33 (± 21)	0.19	8.26×10^7	1.62×10^7	0.20
15250+3609	150 (± 10)	60 (±15)	0.40	4.25×10^7	1.32×10^7	0.31
15462−0450	169 (± 38)	···	···	6.86×10^7	1.90×10^7	0.28
17208−0014	229 (± 15)	110 (± 20)	0.48	2.33×10^8	2.63×10^7	0.11
20087−0308	219 (± 14)	50 (± 15)	0.23	1.94×10^8	3.31×10^7	0.17
20414−1651	187 (± 32)	96 (± 38)	0.51	1.03×10^8	1.82×10^7	0.18
20551−4250	140 (± 15)	40 (± 10)	0.29	3.22×10^7	1.32×10^7	0.41
21219−1757	121 (± 11)	···	···	1.79×10^7	1.51×10^7	0.84
21504−0628	90 (± 31)	9 (± 28)	0.10	5.45×10^6	8.30×10^6	1.52
23230−6926	143 (± 14)	23 (± 13)	0.16	3.50×10^7	1.44×10^7	0.41
23365+3604 [e]	145 (± 15)	···	···	3.71×10^7	1.62×10^7	0.44
23578−5307	190 (± 70)	···	···	1.10×10^8	1.66×10^7	0.15

Note. — The stellar central velocity dispersion, rotational velocity, and the $V_{\rm rot}/\sigma$ ratio are derived from the spectra of Fig. 1 with the aid of the parameters of Table 2. The dynamical and Eddington black hole mass of each ULIRG and the ratio of the two are also presented here.

[a]The observed rotational velocity value presented in this column is corrected for angular deviations from the major axis of rotation but not for inclination effects.

[b]Dynamical black hole masses estimated from their relation to the bulge dispersion (Tremaine et al. 2002).

[c]Eddington black hole mass, calculated by attributing 50% of L_{IR} to the AGN.

[d]Ratio of Eddington over dynamical black hole mass.

[e]The rotational velocity measured by Genzel et al. (2001) for these sources is an upper limit.

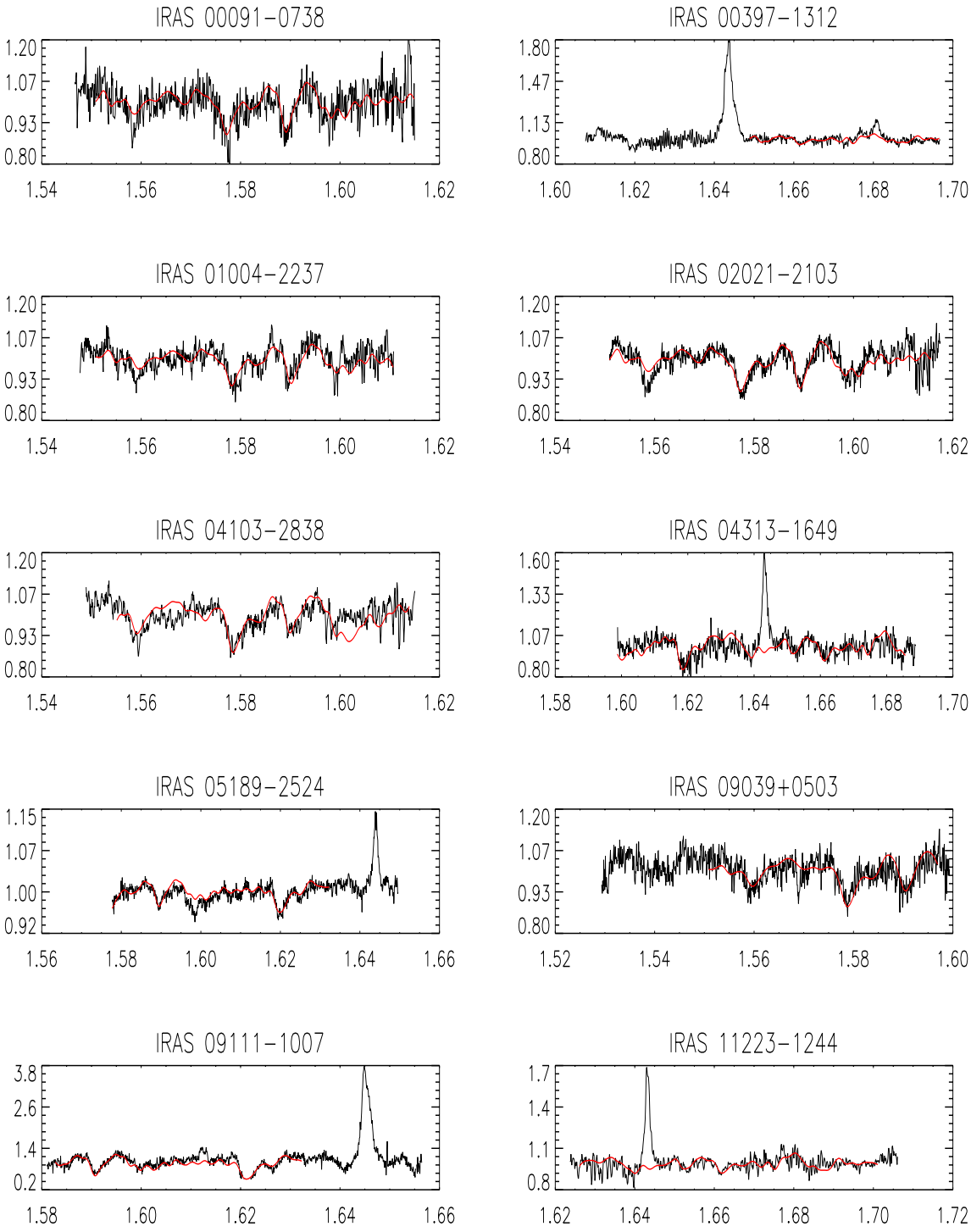

Fig. 1.— The H-band spectra of the ULIRG remnants from this study. The stellar template, convolved with Gaussians that represent the LOS broadening function of the sources, is overplotted as a solid line. All spectra are shifted to rest frame.

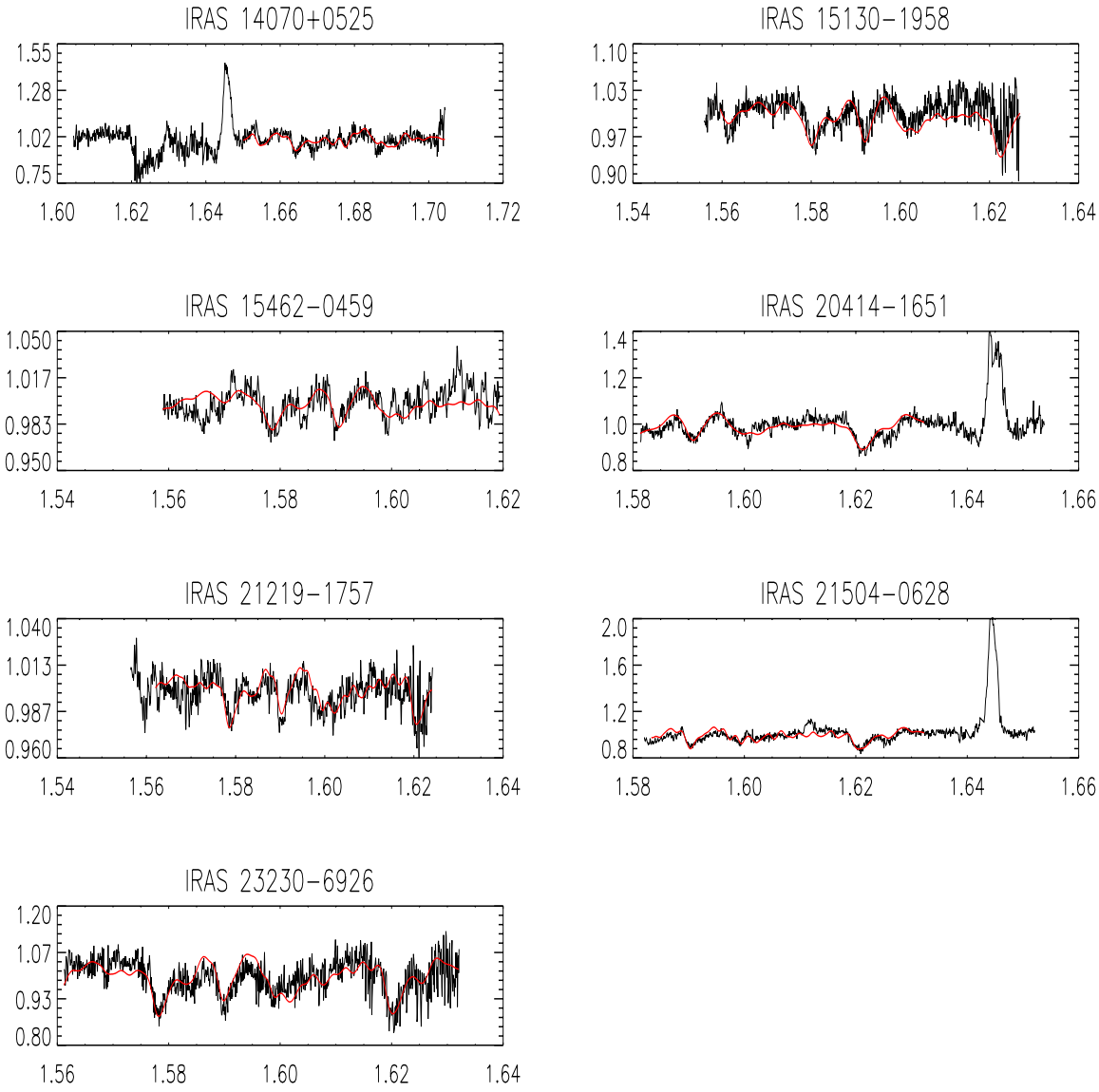

Fig. 1 continued.

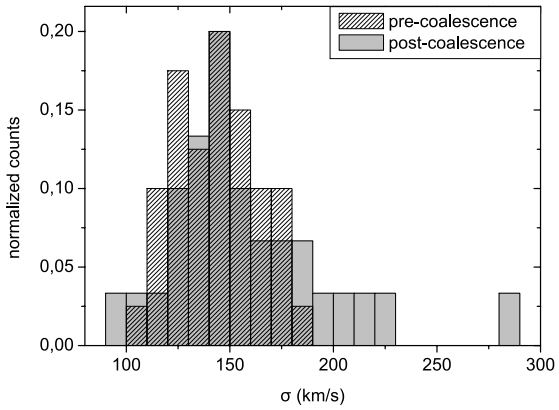

Fig. 2.— The distributions of stellar dispersions in ULIRGs before and after nuclear coalescence.

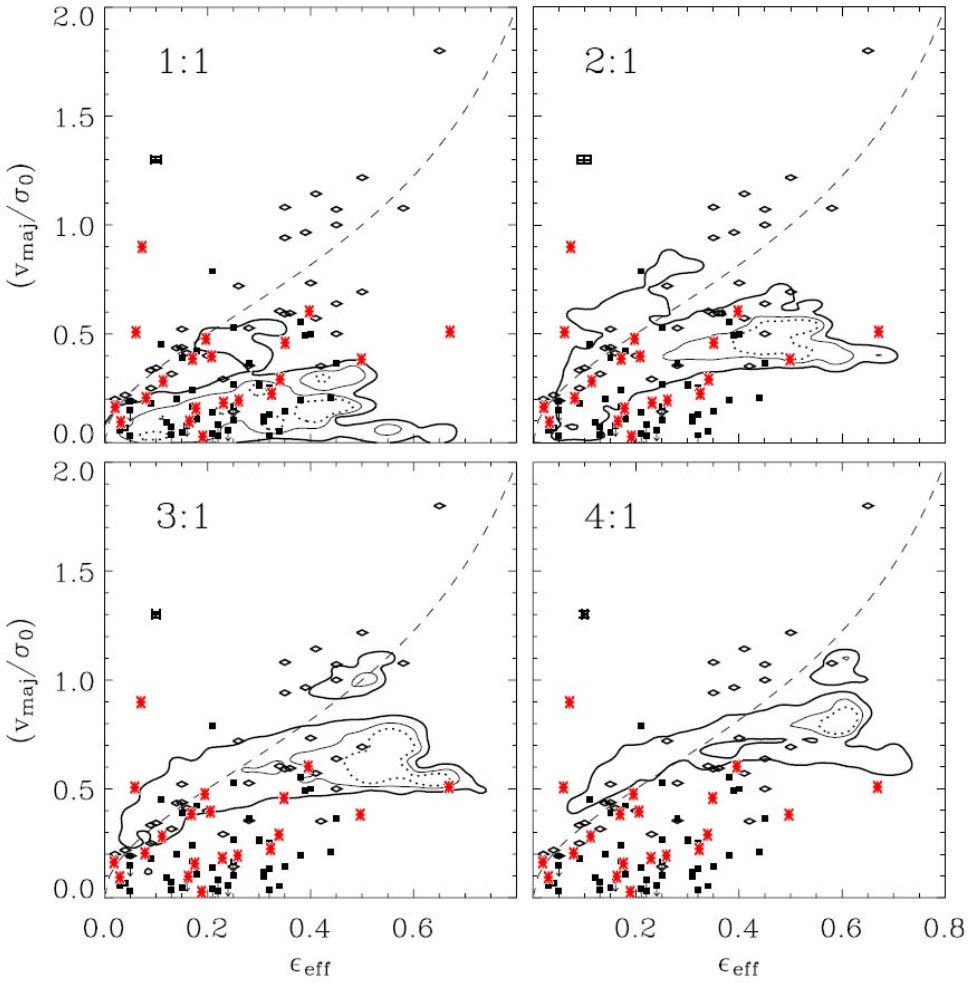

Fig. 3.— Ratio of observed rotational over dispersion velocity versus ellipticity for merger remnants (from Naab & Burkert 2003). Each panel corresponds to mergers of different progenitor mass ratios (cases from 1:1 to 4:1 are studied). The bold line, solid line, and dotted contours indicate the position of the diagram where mergers of each category are expected to be found at 90%,70%, and 50% probability levels respectively. The squares and open diamonds correspond to boxy and disky ellipticals. The dashed line shows the theoretical values for an oblate isotropic rotator. ULIRG remnants are shown as stars.

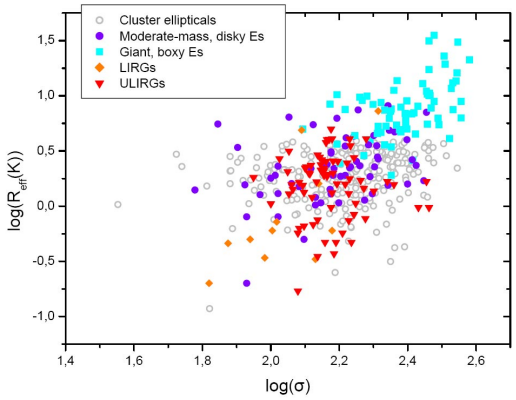

Fig. 4.— The $R_{\rm eff}$-σ projection of the K-band early-type galaxies fundamental plane. The ULIRGs are plotted as triangles. The data for the giant boxy and moderate-mass disky Es (squares and circles respectively) are taken from Bender et al. (1992) and Faber et al. (1997). More (cluster) Es (open circles) are from Pahre (1999) and LIRGs (diamonds) from Shier & Fischer (1998) and James et al. (1999).

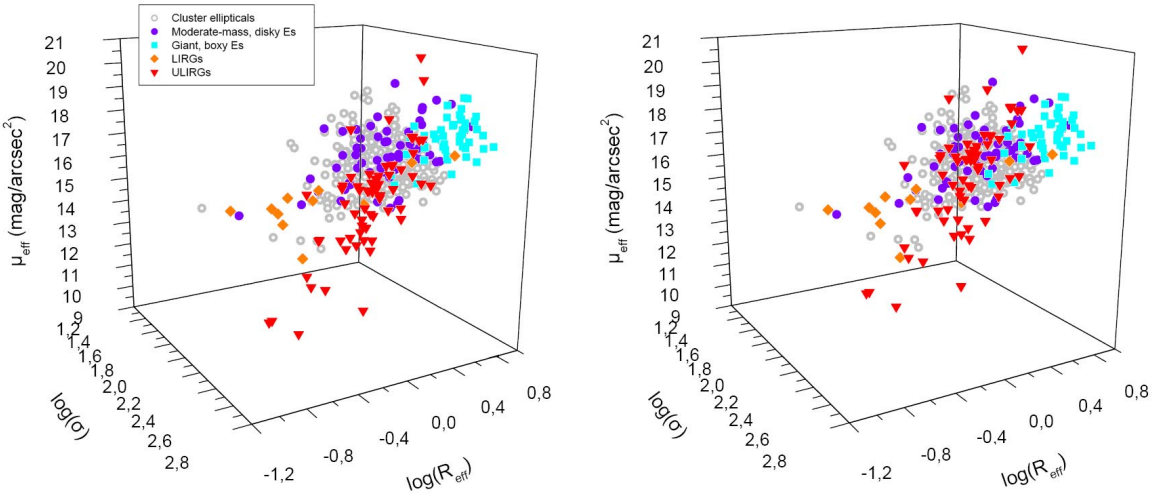

Fig. 5.— The 3-dimensional view of the (K-band) fundamental plane of early-type galaxies. The symbols used are identical to those in Fig. 4. In the left panel we use the magnitudes of Kim et al. (2002), while in the right panel those of Veilleux et al. (2006), where the nuclear PSF has been removed. Extinction corrections have been applied in both cases.

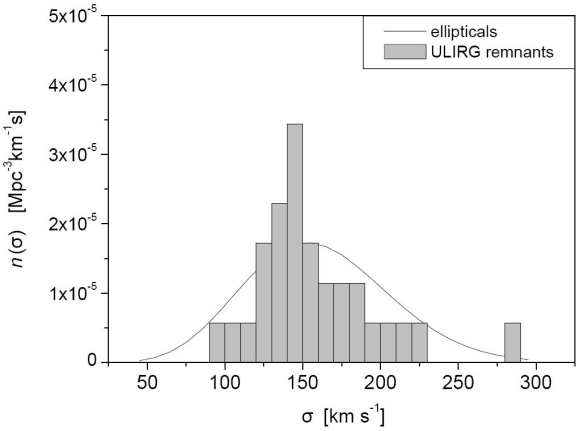

Fig. 6.— The number density of sources as a function of their stellar velocity dispersion is plotted in this figure. The solid line corresponds to the number density per σ of SDSS ellipticals, computed from their dispersion function (Sheth et al. 2003). The number density per σ of ULIRG remnants, plotted as a histogram, is calculated by multiplying the % fraction of our remnants that resides in each σ bin with the local volume density of ULIRGs from Sanders et al. (2003). To facilitate the comparison, the ULIRG histogram is further normalized so that its mean has the same number density as that of the elliptical $n(\sigma)$ distribution.

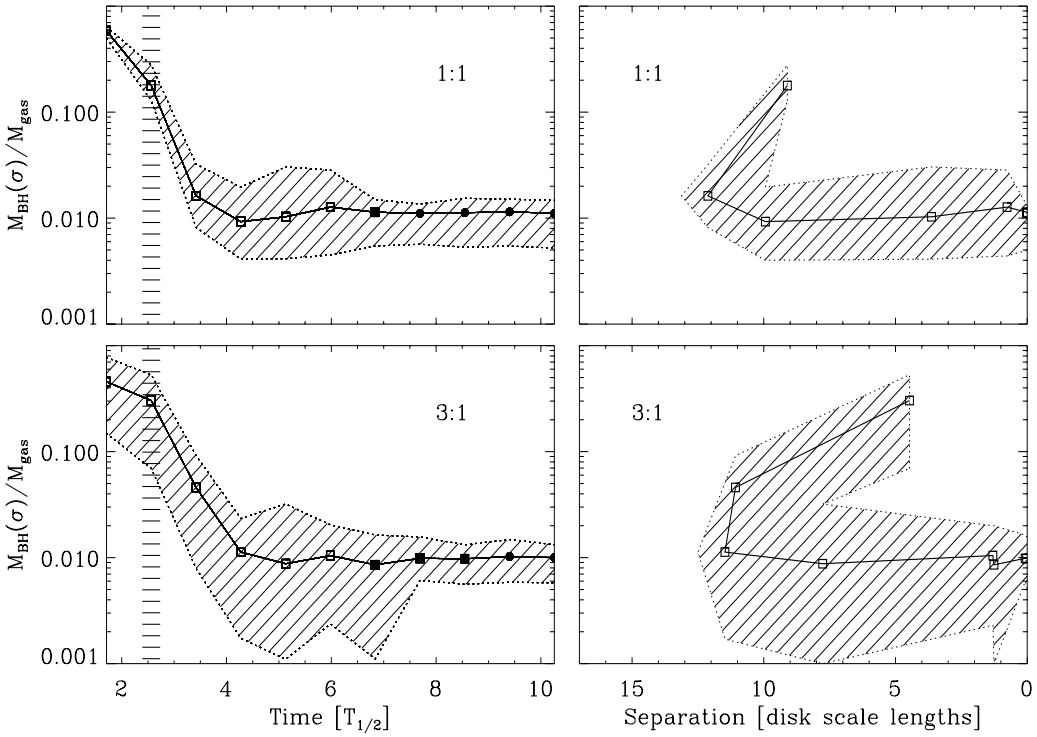

Fig. 7.— Evolution, during a disk-galaxy merger, of the average black-hole mass inferred from the central (line-of-sight) stellar velocity dispersion of the simulated galaxies. The black hole mass is in units of the average total accreted gas mass onto the center of the simulations. In the left column, the evolution is given as a function of time. Time is plotted in units of the half-mass rotation period, $T_{1/2}$, of the more massive progenitor disk. Open squares represent disks that are still separated, filled dots indicate fully merged systems. The spread originating from the initial disk orientations is indicated by the diagonally shaded area. The vertically shaded area indicates the first data point after the first encounter. In the right column, the evolution is plotted as a function of nuclear separation of the interacting galaxies. The nuclear separation unit is the disk scale length h of the more massive disk. Only data points after the first encounter have been plotted. In both columns, 1:1 mergers are shown in the upper and 3:1 mergers in the lower panel.